Journal of Materials Chemistry A

ROYAL SOCIETY OF CHEMISTRY

PAPER

View Article Online
View Journal | View Issue

Cite this: J. Mater. Chem. A, 2024, 12, 17181

Regulating the selectivity through ionomer–catalyst interactions for high-efficiency electrocatalytic CO_2 reduction†

Chen Yu,[a] Taoning Lei,[a] Li Xu,[a] Chuyao Jin,[a] Jundong Yi,[b] Shenghui Liu,[b] Saisai Lin,[a] Yang Yang,[ac] Hao Song,[a] Kaige Wang,[a] Haidong Fan,[b] Chenghang Zheng,[abc] Xiao Zhang *[abc] and Xiang Gao *[ab]

Received 26th April 2024
Accepted 16th June 2024

DOI: 10.1039/d4ta02905d

rsc.li/materials-a

Establishing a suitable electrode microenvironment is important to achieving high-efficiency electrocatalytic CO_2 reduction at industrially relevant current densities. Introducing ionomers provided an effective method for regulating the electrode microenvironment, but the mechanism of interactions between the ionomer and the catalyst remains elusive. In this work, the influence of three types of ionomers on the performance and microenvironment of Ag nanoparticle (NP) and molecularly dispersed cobalt phthalocyanine (CoPc MDE) catalysts were systematically investigated. It was found that the non-covalent interactions between the ionomers with aromatic groups and CoPc MDE resulted in the hydrophilicity of electrode and undesirably promoted the generation of hydrogen during the reaction. The optimal ionomer–catalyst combinations achieved excellent FE(CO)s > 99% at current densities up to -200 mA cm^{-2} and stable operation for more than 180 h at a current density of -100 mA cm^{-2}. This work underlines the necessity of selecting appropriate ionomer according to the nature of catalyst.

1. Introduction

The consumption of fossil fuels has emitted over 35 billion tons of CO_2 globally each year and caused severe climate issues. To reach the Paris Agreement's goal of limiting the global average temperature rise to 2 °C, converting CO_2 into value-added green fuels or chemicals, including CO, formate, methanol, and ethylene, with renewable energy *via* electrocatalytic CO_2 reduction reaction (CO_2RR) is a promising route to reduce CO_2 emission. Among the CO_2 conversion products, CO could serve as a pivotal platform chemical in the chemical industry and be further converted to various valuable chemicals through established techniques, such as Fischer–Tropsch synthesis.[1,2] Compared to the thermocatalytic reverse water–gas shift (RWGS) reaction for CO_2-to-CO conversion usually proceeding at high temperatures,[3] CO_2RR offers significant advantages of mild reaction conditions[4] and direct utilization and storage of renewable energy.[5] To date, great efforts have been devoted to CO_2RR to produce CO, primarily focusing on catalyst design for achieving high faradaic efficiencies (FEs) and minimizing energy cost. Various types of catalysts have been developed for CO production, including metal-based catalysts,[6,7] single-atom catalysts,[8,9] metal-free carbon-based catalysts,[10,11] and molecular catalysts.[12–14]

Although these catalysts exhibited excellent intrinsic CO selectivity with FE(CO)s greater than 95%,[14–16] their CO_2RR performance, especially at industrially relevant high current densities of more than 100 mA cm^{-2}, also heavily relied on enhancing the mass transfer efficiency. Gas-diffusion electrode (GDE) structure, allowing CO_2 to be efficiently transferred to the active sites in gas phase to establish abundant gas–liquid–solid triple phase boundary (TPB), is widely adopted for CO_2RR at high current densities.[17,18] Consequently, regulating the electrode microenvironment and the associated mass transfer process of CO_2 and water becomes a significant issue in preparing GDEs.[19–21] Employing ionomers as binders is a common practice in the preparation of GDEs, and further research indicates that the addition of ionomers can significantly influence the catalytic performance. Specifically, the binding of ionomers with methylimidazolium groups to the Cu catalyst could diminish the adsorption of CO intermediates on the active sites, thereby promoting the generation of CO.[22] It is observed that hydrophilic Cu electrode resulted from the addition of a piperidinium-containing ionomer promotes hydrogen evolution reaction (HER) and formate formation. In addition, Donnan exclusion due to the charged groups within ionomers enables efficient regulation of the pH and the concentrations of H_2O and CO_2 surrounding the Cu catalyst

[a]State Key Laboratory of Clean Energy Utilization, Zhejiang University, Hangzhou, 310027, P. R. China. E-mail: xgao1@zju.edu.cn; zhangx_energy@zju.edu.cn
[b]Baima Lake Laboratory, Hangzhou, 310051, P. R. China
[c]Jiaxing Research Institute, Key Laboratory of Clean Energy and Carbon Neutrality of Zhejiang Province, Zhejiang University, Jiaxing 314000, P. R. China

† Electronic supplementary information (ESI) available. See DOI: https://doi.org/10.1039/d4ta02905d

surface, leading to a high C_{2+} selectivity of up to 90%.[23] MoP nanoparticles modified with imidazolium ionomer could enhance CO_2 diffusion in the catalyst layer and increase local CO_2 concentration near the catalyst, boosting CO adsorption, promoting C–C coupling, and raising ethanol yield.[24] Furthermore, the distribution of ionomer within the catalyst layer also affects the catalytic performance of the catalyst. A pre-confinement method is proposed to prepare GDEs with uniformly distributed ionomer, resulting in low cell voltages and high FE(CO)s across a wide range of current densities even at low CO_2 partial pressures.[25] Although the impact of ionomers on certain CO_2RR catalysts has been studied in some work, the mechanism of interactions between different catalysts and different ionomers and the impacts on their CO_2RR performances were still elusive.

In this study, we systematically examined the influences of three commonly used ionomers, namely one perfluorinated sulfonic-acid (PFSA) cation-exchange ionomer and two methylimidazolium- and piperidinium-containing anion-exchange ionomers, on the CO_2RR performances of two representative types of CO producing catalysts, namely Ag NPs and molecularly dispersed cobalt phthalocyanine on nanocarbon materials (CoPc MDE). Distinct surface morphology and hydrophobicity/hydrophilicity of the GDEs were observed with different combinations of ionomers and catalysts, subsequently influencing their CO_2RR activity and selectivity. The Ag NPs mixed with different ionomers showed slight difference in CO_2RR performance, while the hydrophobicity characters and CO selectivity of CoPc MDEs were significantly altered due to the non-covalent interactions between the graphitized nanocarbon materials and the ionomers containing aromatic groups revealed by Raman spectroscopy. In addition, *operando* infrared spectroscopy indicated that the addition of different ionomers to the same catalyst could regulate the electrode microenvironment and significantly change the resulting CO_2RR performance. As ionomers are widely used as binders in preparing electrodes, this work could provide valuable insights for choosing the appropriate ionomers for CO_2RR systems.

2. Experimental

2.1 Materials

Silver nanoparticles (20 nm particle size, 99.99% trace metals basis) were purchased from Shanghai Maoguo. CoPc (95% purity), Nafion 117 (~5% in a mixture of lower aliphatic alcohols and water), isopropanol (chromatographic grade, 99.8%), *N*,*N*-dimethylformamide (>99.9%, GC), nano-graphite powder (99.95% metals basis), and ethanol (anhydrous grade, ≥99.5%) were purchased from Aladdin. KOH (ACS reagent, ≥85%) and $KHCO_3$ (ACS reagent, 99.7%) were purchased from Sigma-Aldrich. Carbon nanotubes (CNT) (CR05-G, multi-walled, ash content ≤ 0.3%) were obtained from Qingdao Chaorui Nanotech. Carbon-based GDL (YLS-30T), methylimidazolium ionomer powder (Sustainion XA-9, dispersed in isopropanol at 5 wt% for use), and piperidinium ionomer solution (PiperION-A5) were purchased from Suzhou Sinero Technology. CO_2 (99.999%) and N_2 (99.999%) were purchased from Hangzhou Jingong. PTFE particles (100 nm) were purchased from Kexinda Polymer Materials. All chemicals were used as received without further purification. Ultra-pure water with a resistivity of 18.2 MΩ cm at 25 °C was used throughout the experiments.

2.2 Preparation of CoPc MDE

To prepare CoPc MDE, 30 mg of CNTs (CR05-G) were dispersed in 20 ml of DMF using high-power ultrasonication (Xiaomei XM-08II, 1800 W) for 1 hour. 3 mg of CoPc was dispersed in another 10 ml of DMF with ultrasonication and then added to the CNT suspension. The mixed suspension was further ultrasonicated for 1 hour and stirred at room temperature for 24 hours. The solid was separated by centrifugation and washed with DMF, ethanol, and water. Finally, the product was freeze-dried to obtain CoPc MDE.[15] CoPc supported on nano-graphite powder was prepared by the same procedure above with nano-graphite powder replacing CNTs.

2.3 Preparation of catalyst ink and GDE

5 mg of catalyst powder and 5 mg of PTFE particles were dispersed in 2.25 ml of isopropanol and mixed with a calculated volume of ionomer solution by ultrasonication for 1 h. The addition of PTFE particles could enhance the diffusion of CO_2 to the active site.[15] 1.6 ml of catalyst ink was drop-coated onto a 3 × 1.2 cm^2 GDL to reach a catalyst loading of 1 mg cm^{-2}. The GDE was heated on a heating plate at 40 °C to facilitate solvent evaporation.

2.4 Assembly of the electrolyser

A homemade three-compartment (gas chamber, cathode chamber, and anode chamber) flow cell with a working area of 1 (2 × 0.5) cm^2, which was described in detail previously,[17] was used for the three-electrode GDE experiments. The cathode chamber and anode chamber were separated by a Nafion 117 ion exchange membrane (a bipolar membrane, Fumasep FBM-PK, was used in stability tests). 1 M $KHCO_3$ and 2 M KOH solutions were used as the catholyte and anolyte, respectively. Nickel mesh and Ag/AgCl (saturated KCl solution) electrode (inserted into the cathode chamber) served as the anode and reference electrode, respectively. A homemade three-compartment flow cell with a working area of 25 (5 × 5) cm^2 was also assembled. Nickel foam was used as the anode. The cathode chamber and anode chamber were separated by a Nafion 117 ion exchange membrane during the testing process. All the other procedures were the same as those for the 1 cm^2 flow cell.

2.5 Electrochemical measurements

All electrochemical measurements were carried out with a CHI 760E potentiostat and a Princeton PMC potentiostat (for impedance measurements). A three-electrode configuration was used for CO_2RR measurements. All potentials were recorded against an Ag/AgCl (saturated KCl solution) reference electrode and converted to *versus* RHE with 85% *iR* compensation using the following equation:

$$E_{RHE} = E_{Ag/AgCl} + 0.0591 \times pH + 0.197 - iR_u \times 85\%$$

where i is the current and R_u is the solution resistance.

CO_2 was delivered into the gas chamber of the electrochemical cell at a flow rate of 20 sccm for reaction (350 sccm in large-scale device), followed by entering the headspace of the catholyte bottle. After leaving the catholyte bottle, the gas stream mixed with N_2 (as an internal standard to eliminate the impact of gas volume change during reaction on product quantification: N_2 flow rate of 9 sccm for 1 cm^2 device experiments and 30 sccm for 25 cm^2 device experiments, respectively) in a gas mixing device, which was then delivered to the sampling loop of an online gas chromatograph (GC) for product quantification. By conducting electrocatalytic tests under constant current densities, gas-phase samples were measured for three times by GC with a 15 minutes interval to obtain the FEs of gas-phase products. To activate the CoPc MDE electrodes, a current density of -10 mA cm^{-2} was applied for 40 min prior to the reaction.

2.6 Product analysis

A GC (Fuli 9790Plus) equipped with a thermal conductivity detector (TCD) and a flame ionization detector (FID) was used for quantitative analysis of gas-phase products. The FID with a methanizer was used for quantifying the CO concentration and the TCD was used for quantifying the H_2 and N_2 concentrations. The responses to different gases were calibrated with standard gas mixtures. The calculation of FE(H_2)s and FE(CO)s was performed using the following equation:

$$FE(g) = \frac{f_x \times A_x \times V_{N_2} \times n \times F}{f_{N_2} \times A_{N_2} \times V_m \times i} \times 100\%$$

where f_x and f_{N_2} are the correction factors for CO/H_2 and N_2, x can be represented as either CO or H_2; A_x and A_{N_2} are the peak areas of CO/H_2 and N_2 measured by the GC; V_{N_2} is the flow rate of N_2; n represents the number of electrons required for the generation of one CO/H_2 molecule; F is the Faraday's constant; V_m is the molar volume of the standard gas; i is the applied current of the reaction.

Formate ($HCOO^-$) in the catholyte was measured using an ICS-900 ion chromatograph (IC). Methanol (MeOH) was measured using an Agilent 7890A GC. The calculation of FE($HCOO^-$) and FE(MeOH) was performed using the following equation:

$$FE(l) = \frac{C \times V \times n \times F}{Q} \times 100\%$$

where C represents the measured concentration of formate or methanol; V is the volume of the catholyte; n is the number of electrons transferred for formate or methanol generation; F is the Faraday's constant, and Q is the total charge transferred during the reaction.

3. Results and discussion

3.1 Preparation and characterizations of GDEs

Ag NPs and CoPc MDE were chosen as the representative catalysts in this work for CO_2RR to CO due to their high activities and selectivity.[12,26–30] Nafion 117,[31,32] Sustainion XA-9,[33] and PiperION-A5 (ref. 25) were selected as ionomers (see Fig. 1 for their structures). Nafion 117 (abbreviated as N), a perfluorinated sulfonic acid ionomer, was a popular choice because of its outstanding chemical stability and high ion conductivity. Sustainion XA-9 (abbreviated as S), an anion-exchange ionomer with methylimidazolium groups, was chosen due to the reported excellent performance in CO_2RR systems.[34] PiperION-A5 (abbreviated as P), another anion-exchange ionomer containing piperidinium groups, was demonstrated to have remarkable performance in fuel cell applications due to the ample ion conductivity and chemical stability.[35] The electrocatalytic performance was subjected to the electrode microenvironment and mass transport regulated by ionomers.[36–41]

Catalyst inks were first prepared and their dispersion was improved with the introduction of ionomers, evidenced by the ability to maintain the initial form for an extended duration (Fig. S1†). The GDEs prepared with Ag NPs and CoPc MDE exhibited distinct morphologies (Fig. 2, S2 and S3†). Ag NPs (~20 nm) were interspersed with PTFE particles (~100 nm), while in CoPc MDE, PTFE were adhered onto CNTs. This observation was further confirmed by energy dispersive spectroscopy (EDS) elemental mappings (Fig. S4 and S5†). The distribution of F elements overlapped with that of Ag and C elements. The surface morphologies were varied with different catalyst–ionomer combinations. The agglomeration of Ag and PTFE particles was observed with the addition of ionomers in Ag–N, Ag–S, and Ag–P GDEs. In addition, PTFE formed larger block structures in Ag–N and Ag–P. Similarly, differences of surface morphologies were observed in CoPc MDE mixed with different ionomers. A large number of pore structures were shown in CoPc MDE-N, which was similar to CoPc MDE. However, the CoPc MDE-S and CoPc MDE-P exhibited smooth and dense structures with much less pores, which also supported the enhanced dispersibility of CoPc MDE in the inks containing the anion-exchange ionomers.

3.2 CO_2RR performance in flow cell

The mass transfer of CO_2 was enhanced in GDE during the reaction process, leading to higher partial current density of CO_2RR in the flow cell compared with that in the H-cell (Fig. S6†). The performance of different GDEs were assessed by analyzing the products after reaction at a current density of -150 mA cm^{-2}. An internal standard method for gas-phase product quantification was employed through mixing the gas flow from the flow cell with N_2 at certain flow rate before entering the sample loop of the GC (Fig. 3a). This modified method could reduce the error due to the change in the total gas flow rate at the gas chamber outlet during reaction and get more accurate gas-phase data compared with the conventional method.[42] The FE(CO), FE(H_2), and FE($HCOO^-$) of Ag NPs without the addition of ionomer were 94.8%, 1.0%, and 1.9%, respectively (Fig. 3b), in line with the reported performance of Ag catalysts.[43,44] Changes of the selectivity for the products were observed upon incorporation of the three ionomers. For Ag–N, the FE of H_2 and formate were slightly increased to 3.6% and

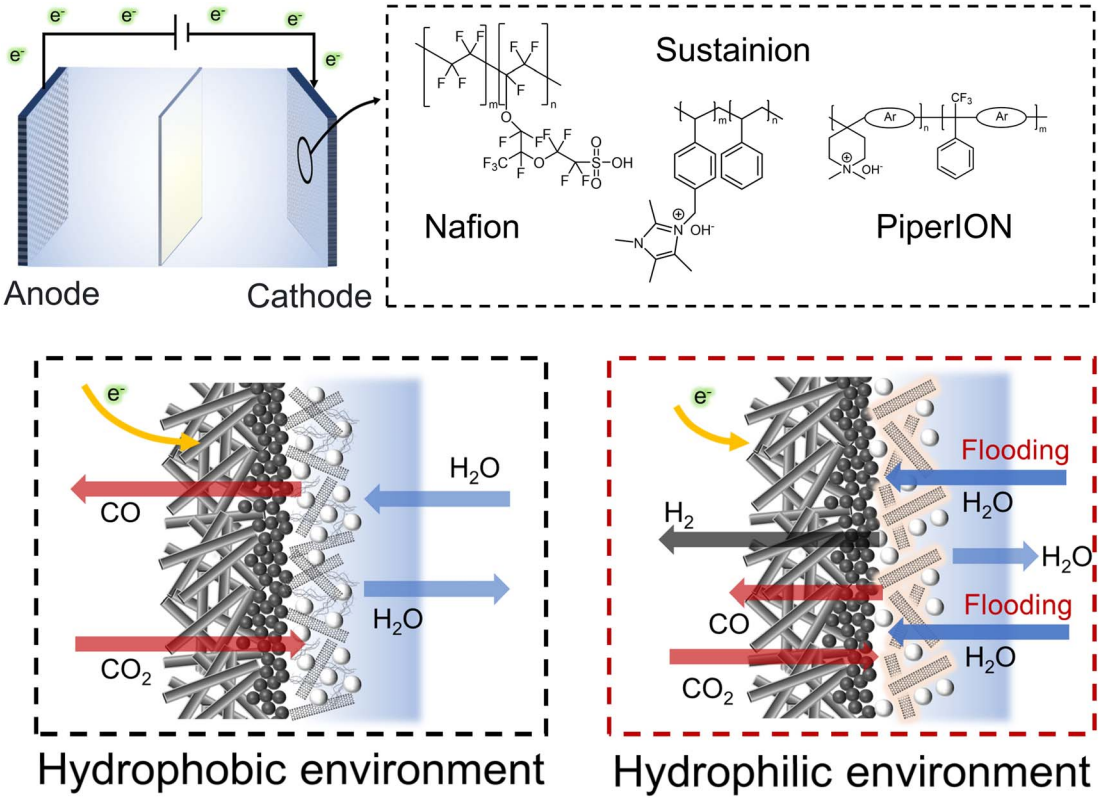

Fig. 1 The chemical structures of the ionomers and the influence on the electrode microenvironment. The electrode microenvironment could be changed with the introduction of ionomers. A hydrophobic environment could establish abundant gas–liquid–solid triple phase boundary (TPB) for CO_2RR, while a hydrophilic environment could lead to flooding of the GDE and increase H_2 generation rate.

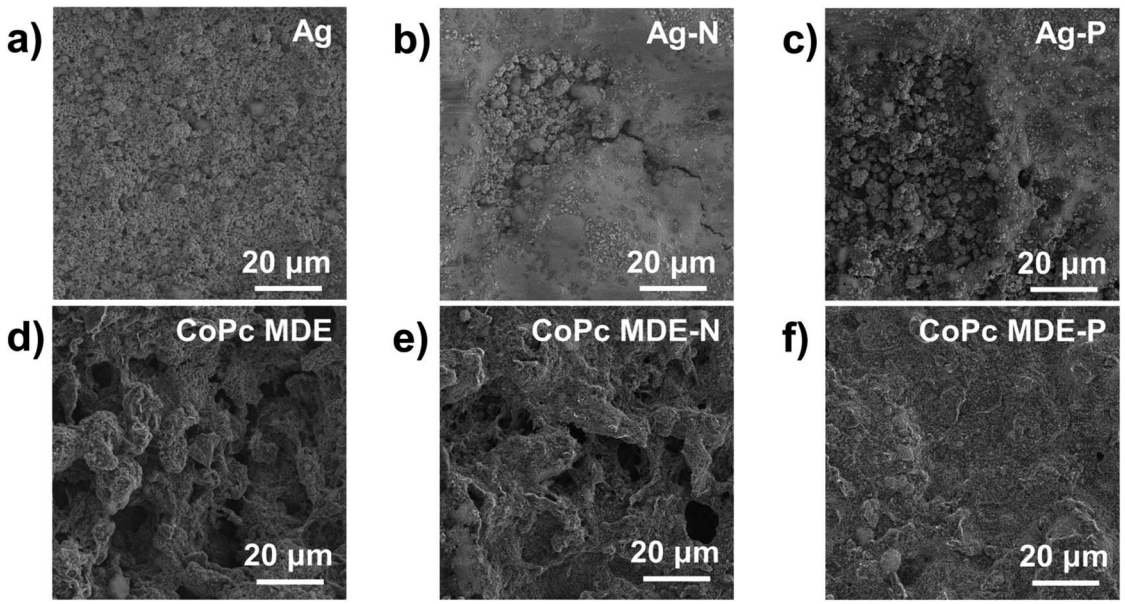

Fig. 2 SEM images of the catalytic layer of the GDEs. (a) Ag, (b) Ag–N, (c) Ag–P; (d) CoPc MDE, (e) CoPc MDE-N and (f) CoPc MDE-P.

3.9%, respectively. Ag–S exhibited similar FE(H_2) to that of Ag and the FE($HCOO^-$) increased to 6.6%. However, a high FE(H_2) of 15.9% was obtained with Ag–P. The variations of the product selectivity induced by different ionomers were more pronounced in the CoPc MDE electrodes (Fig. 3d). The FE(CO) of CoPc MDE was 98.1%, which was further increased to 99.8% in CoPc MDE-N. However, CoPc MDE-S and CoPc MDE-P exhibited severe HER with FE(H_2)s greater than 40%.

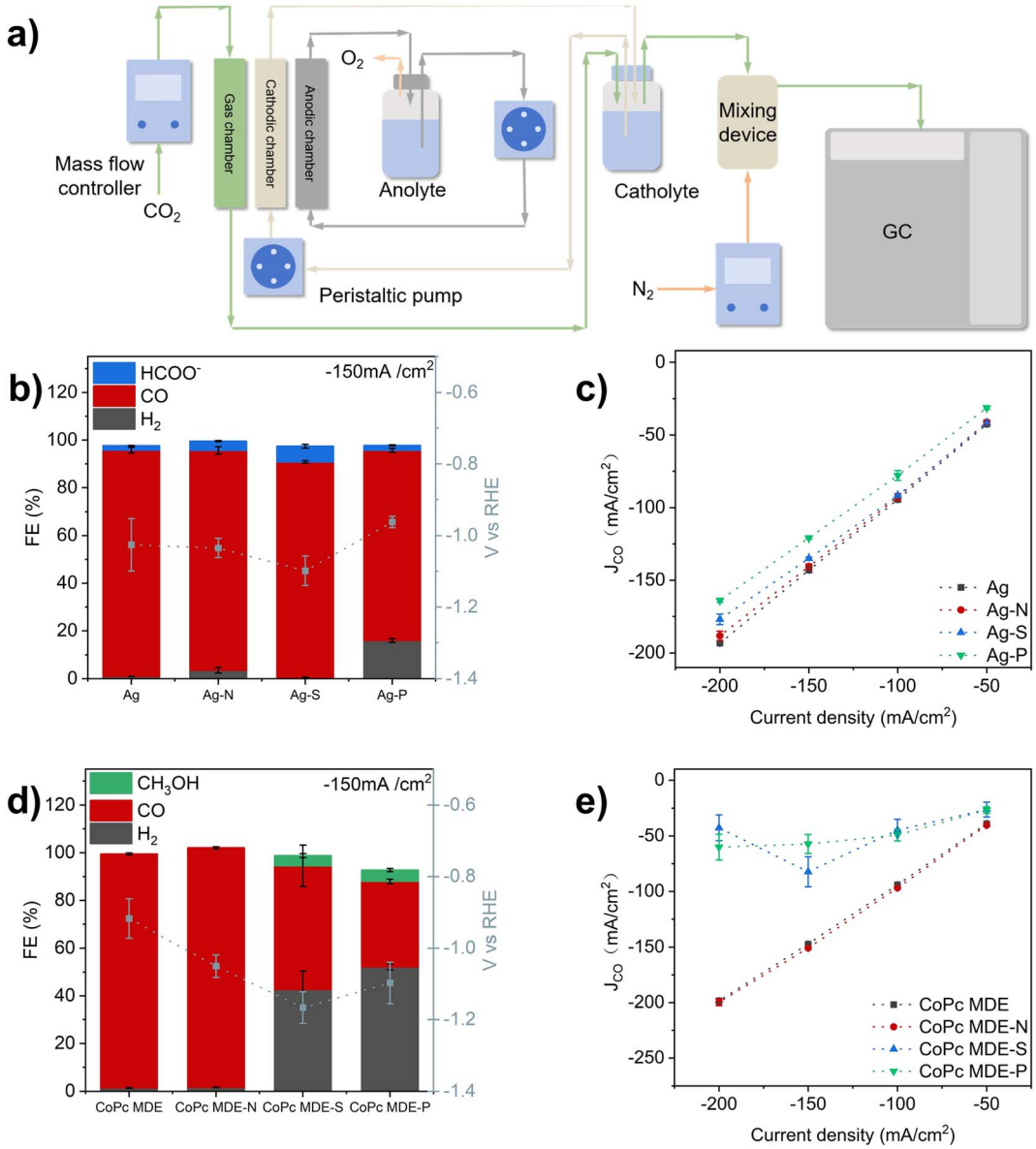

Fig. 3 Schematic presentation of the CO_2RR testing system and the performance of GDEs with different catalyst–ionomer combinations. (a) Schematic illustration of the nitrogen internal standard. The FEs of (b) Ag and (d) CoPc MDE system. The partial current density of CO in the (c) Ag system and (e) CoPc MDE system. The ionomer contents were 10 wt% in all measurements.

Noteworthy, CoPc MDE-S and CoPc MDE-P had a small amount of methanol generated during CO_2RR (4.2% and 4.8%, respectively), which was attributed to the surface-bound CO on the catalyst undergoing further reduction, leading to the formation of methanol. Utilizing CoPc catalysts to reduce CO_2 to methanol was reported in the previous literature, and the reduction process involved the sequential steps of CO_2-CO-MeOH.[45,46] Under various current density conditions, partial current densities of CO and H_2 were plotted for the GDEs. The high activity for CO_2RR was shown in Ag with high CO partial current densities up to -193 mA cm^{-2} at applied current density at -200 mA cm^{-2}, whereas Ag–P consistently exhibited high H_2 partial current density (Fig. 3c and S7a†). The addition of anion-exchange ionomer caused the decrease of CO_2RR activity in CoPc MDE system. Higher HER activities were obtained with CoPc-P and CoPc-S at various current densities compared with CoPc MDE and CoPc MDE-N (Fig. S7b†). The poorer performance of Ag–P was attributed to the reduced exposure of active sites due to the agglomeration of Ag NPs. In the case of CoPc MDE-S and CoPc MDE-P, the denser catalytic layer could induce insufficient CO_2 supply at higher current densities, leading to more severe HER and low CO selectivity.

The impact of the ionomer content on the performance of Ag NPs was illustrated in Fig. 4. A slight increase in the FE(H_2)s of Ag–N was observed from 0 to 10 wt% Nafion. This insignificant change was attributed to the excessive addition of Nafion, which caused the active sites of the Ag catalyst enveloped and the decrease of FE(CO)s. The Ag–S electrodes with different

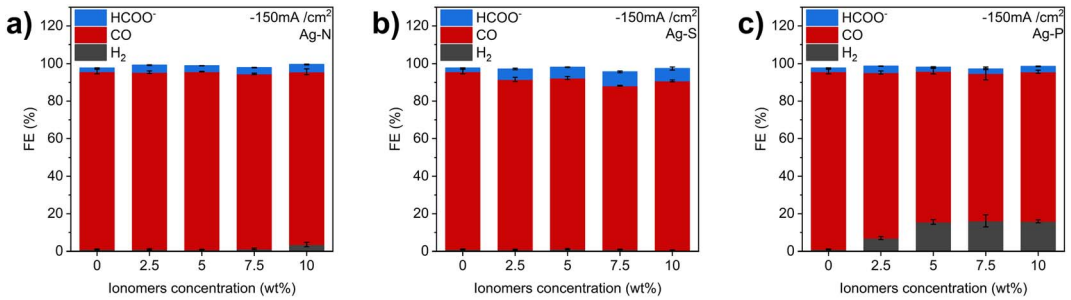

Fig. 4 Product distributions of (a) Ag–N, (b) Ag–S, and (c) Ag–P GDEs with different ionomer contents at a current density of −150 mA cm^{-2}.

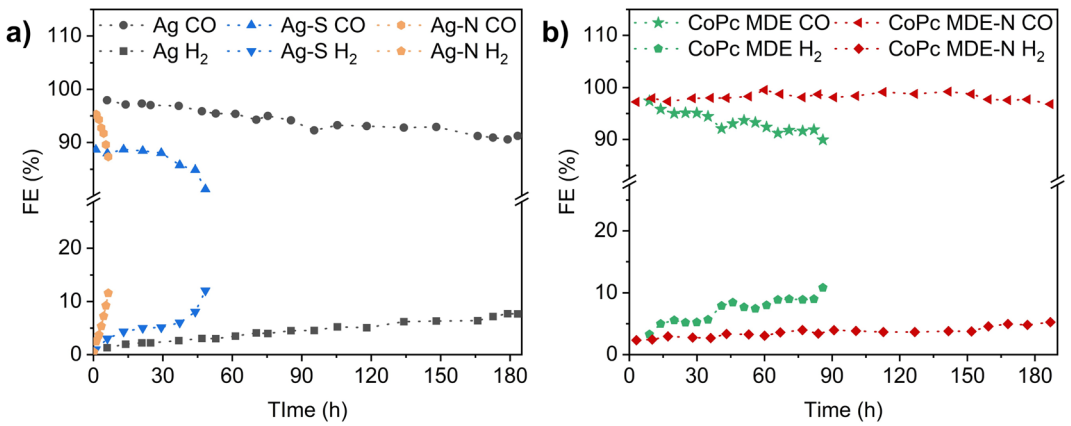

Fig. 5 Long-term stability tests for (a) Ag and (b) CoPc MDE electrodes at a current density of −100 mA cm^{-2}.

ionomer contents maintained low FE(H_2)s and no significant change was observed for the FE($HCOO^-$)s across the measured ionomer contents. Meanwhile, a significant impact on catalytic performance was observed in Ag–P. The maximum FE(H_2) reached 15.6% at ionomer content of 5 wt%, which was not further increased with higher contents. In addition, the CoPc MDE-N electrode demonstrates good performance at all concentrations (Fig. S8†). In contrast, poor CO_2RR activities were observed in CoPc MDE-S and CoPc MDE-P even at ionomer contents as low as 2.5 wt% (Fig. S9†).

The effect of ionomers on the long-term stability of GDEs was evaluated for Ag, Ag–S, Ag–N, CoPc MDE, and CoPc MDE-N because of their demonstrated excellent performance (Fig. 3). However, significant differences were revealed during long-term operation (Fig. 5). For the Ag–S electrode, FE(H_2)s gradually increased during the first 37 h and then increased at a higher rate to 12.1% at 48 h. Ag GDE without the addition of ionomer exhibited better stability and maintained good performance over 180 h at a current density of −100 mA cm^{-2}. Although Ag–N exhibited good selectivity for CO production in short-term measurements, the performance decays with FE(H_2) increasing rapidly from 1.2% to 11.6% within only 7 h. In contrast, CoPc MDE-N showed superior CO_2RR stability compared to CoPc MDE, which maintained high FE(CO)s greater than 95% for nearly 190 h. In contrast, the FE(CO)s of CoPc MDE dropped to below 90% at 86 h. It was worth noting that these stability tests were conducted without any treatment during the reaction (such as washing the electrode or changing the electrolyte). According to the SEM images in Fig. S11,† more Ag NPs fell off from the Ag–S electrode compared with Ag GDE, which might be the reason for worse stability of Ag–S. The addition of Nafion allowed CoPc MDE-N to retain more PTFE particles in the reaction (Fig. S12†). Thus, the superior stability of CoPc MDE-N compared to CoPc MDE could be attributed to maintaining the surface morphology of and preserving the integrity of three-phase boundary with the addition of Nafion ionomer, ensuring an adequate supply of CO_2.

CoPc MDE-N electrodes with a large active area of 25 cm^2 were prepared and assembled in a customized flow cell to evaluate their CO_2RR performance (Fig. 6a). The potential and selectivity of CoPc MDE-N at different current densities in the 25 cm^2 active area flow cell were illustrated in Fig. 6b and c. The FE(CO)s were 96.2% and 96.8% at current densities of −100 mA cm^{-2} and −200 mA cm^{-2}, respectively and slightly decreased to 94.8% at the current density of −250 mA cm^{-2}. The observation of nearly 100% total FE in the 25 cm^2 device testing also demonstrated the reliability of using the nitrogen internal standard method for the determination of reduction products. Furthermore, CoPc MDE-N maintained high FE(CO)s over 95% for 5 h continuous CO_2 electrolysis at a total current of −2.5 A. The successful operation of CoPc MDE-N in the 25 cm^2 flow cell indicated its potential for industrial applications.

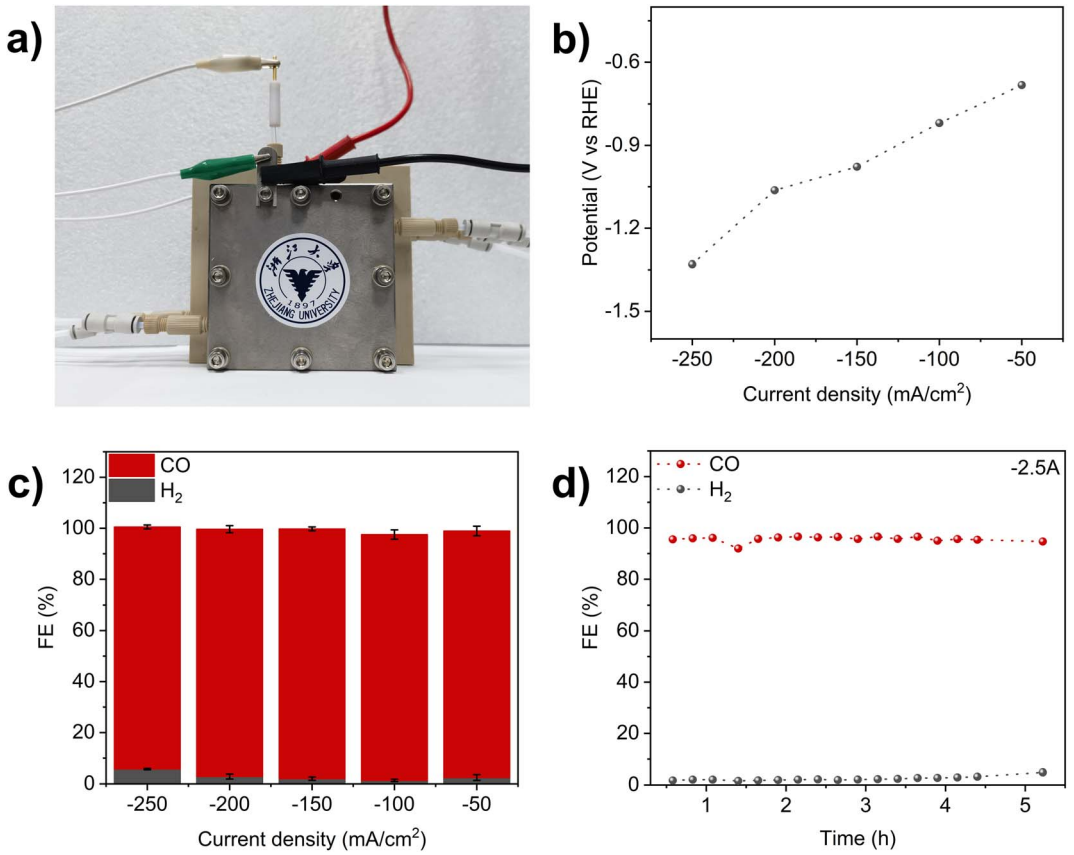

Fig. 6 The performance of CoPc MDE-N in a 25 cm^2 flow cell. (a) Digital photograph of the 25 cm^2 flow cell. (b) Potential and (c) FEs of CoPc MDE-N at different current densities in the 25 cm^2 flow cell. (d) Long-term stability tests of CoPc MDE-N at −2.5 A in 1 M $KHCO_3$.

4. Mechanism of the ionomer effects

The fundamental reasons for the impact of different ionomers on the selectivity of the GDEs were explored from aspects such as surface hydrophobicity, electrochemical active surface area (ECSA), and charge transfer rate. The hydrophilicity/hydrophobicity of the electrode was influenced to varying degrees after the addition of different ionomers for different catalysts. There was no obvious change of the contact angle in Ag GDEs after adding the Sustainion and Nafion ionomers. Meanwhile, the contact angle of the Ag–P electrode slightly decreased (from 147° to 131°) after the addition of PiperION (Fig. 7a). The hydrophobicity of the electrode was increased by the addition of Nafion to the CoPc MDE electrode. In contrast, for CoPc MDE-S and CoPc MDE-P, a suitable hydrophobic environment for CO_2RR was not provided. Constructing a suitable hydrophobic environment on the electrode surface can greatly enhance the performance of the electrode.[47] Therefore, the hydrophilic surfaces of CoPc MDE-S and CoPc MDE-P were found to be the cause of their inferior CO_2RR performance.

The ECSA tests were used to evaluate potential differences of the active surface area due to variations in electrode surface morphology. At the same time, a larger ECSA may potentially enhance catalytic performance.[48] Surprisingly, the ECSA of Ag and CoPc MDE electrodes exhibited trends that are opposite to their catalytic performance. Although Ag–S and CoPc MDE-N exhibited good catalytic performance and with higher specific surface area measured by N_2 adsorption method (Fig. S15†), they showed lower ECSA (Fig. 7c and d). This difference was due to the increased hydrophobicity reduced the contact between the electrode surface and the electrolyte, thereby the electrochemical double-layer capacitance was decreased.[49] Worthy of mention, despite the lowest ECSA, excellent CO_2RR performance was still obtained by Ag–S, possibly attributed to the enhanced CO_2 adsorption and improved CO_2 availability facilitated by the Sustainion ionomer.[24] The effect of ionomer on the charge transfer resistance was measured through electrochemical impedance spectroscopy (EIS) and was displayed in Fig. S16.† The arcs observed in the low-frequency range were not included in the fitting at this stage, which might be linked to the diffusion of ions in the solution and bicarbonate acting as a proton donor.[50] The noticeable influence of ionomer addition on the charge transfer resistance of the Ag system was observed. Compared to the other three electrodes, Ag–S exhibited a larger charge transfer resistance. This phenomenon could be attributed to the uneven distribution of ionomers caused by simple mechanical mixing, leading to increased charge transfer resistance due to aggregated ionomers.[25] However, a less pronounced effect on the R_{ct} of CoPc MDE system was observed with the addition of ionomers (Table S1†), which was attributed to the well-conductive catalytic layer formed by the intertwining of carbon nanotubes.

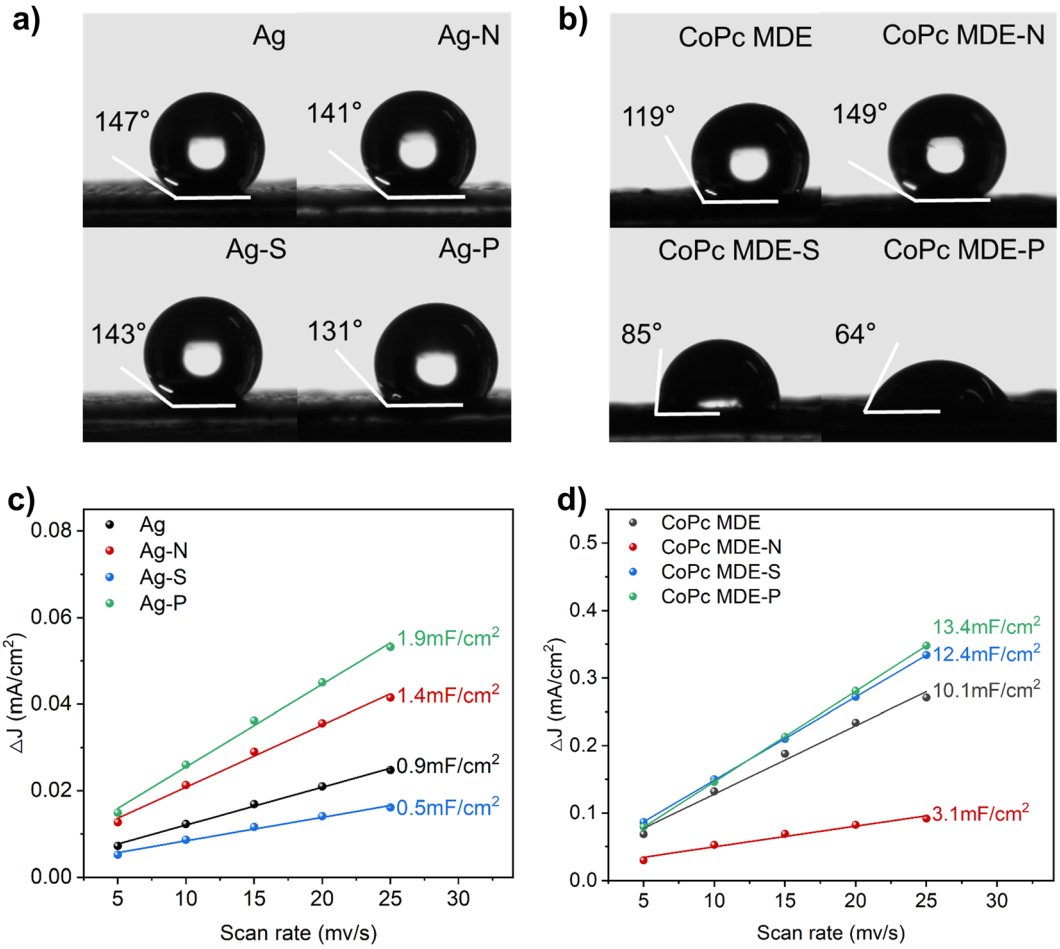

Fig. 7 Contact angle and ECSA of the GDEs. Water contact angles for (a) Ag system and (b) CoPc MDE system. ECSA for (c) Ag and (d) CoPc MDE system.

The significant change on the CO_2RR performance of the CoPc MDE system was observed with adding the ionomers. Further, *operando* attenuated total reflection surface enhanced infrared spectroscopy (ATR-SEIRAS) tests were used to gain deeper insights into the impact of ionomers on the electrode microenvironment and the reaction intermediates of the catalytic layer. As depicted in Fig. 8, the peak near 1650 cm^{-1} was attributed to the O–H bending vibration in adsorbed water molecules under an applied potential. The comparison of water peak signal intensity for CoPc MDE, CoPc MDE-N, and CoPc MDE-S at −0.8 V was illustrated in Fig. S17.† Water signal was shown more obviously in CoPc MDE-S compared with CoPc MDE and CoPc MDE-N. This finding was aligned with the results of the contact angle tests. The low solubility of CO_2 in water results in poor contact between CO_2 and the catalyst in hydrophilic electrodes such as CoPc MDE-S and CoPc MDE-P. Insufficient CO_2 supply led to inferior catalytic performance, as reported in previous literature.[51] Additionally, the *COOH intermediate was detected near 1409 cm^{-1},[16,52,53] which was increased with applied potential and indicated the accelerated generation of CO. The peak at 1913–1936 cm^{-1} was attributed to adsorbed CO on the active sites,[54,55] with the shift in peak position due to the Stark effect.[56] The signals of *COOH and *CO intermediates were also observed in CoPc MDE-N (Fig. S18†). Notably, the *CO peak was not detected in the CoPc MDE-S, which was potentially caused by the excessive hydrophilicity of the GDE, leading to the dominant presence of HER during the test and posing challenges in detecting intermediates of the CO_2RR. The regulation of different ionomers on the electrode microenvironment was reflected in the influence on the water content of the catalyst layer and the activity of the catalyst was improved by creating an appropriate hydrophobic environment.

It was quite peculiar that in different catalyst systems, the same ionomer (*e.g.*, Sustainion) led to completely opposing catalytic performances. The addition of Sustainion resulted in inferior CO_2RR performance of CoPc MDE-S, even though excellent CO selectivity was observed in CoPc MDE. During the preparation of CoPc MDE, CoPc was uniformly anchored onto the carbon nanotubes on the nanoscale due to π–π interaction between CoPc and CNT. This kind of π–π interaction has been utilized for modification of graphene/carbon nanotubes, improving their solubility and dispersibility in polar solvents.[57–59] It was hypothesized that the aromatic rings in Sustainion XA-9 and PiperION A5 ionomers could interact with carbon nanotubes in a similar way, resulting in coating the

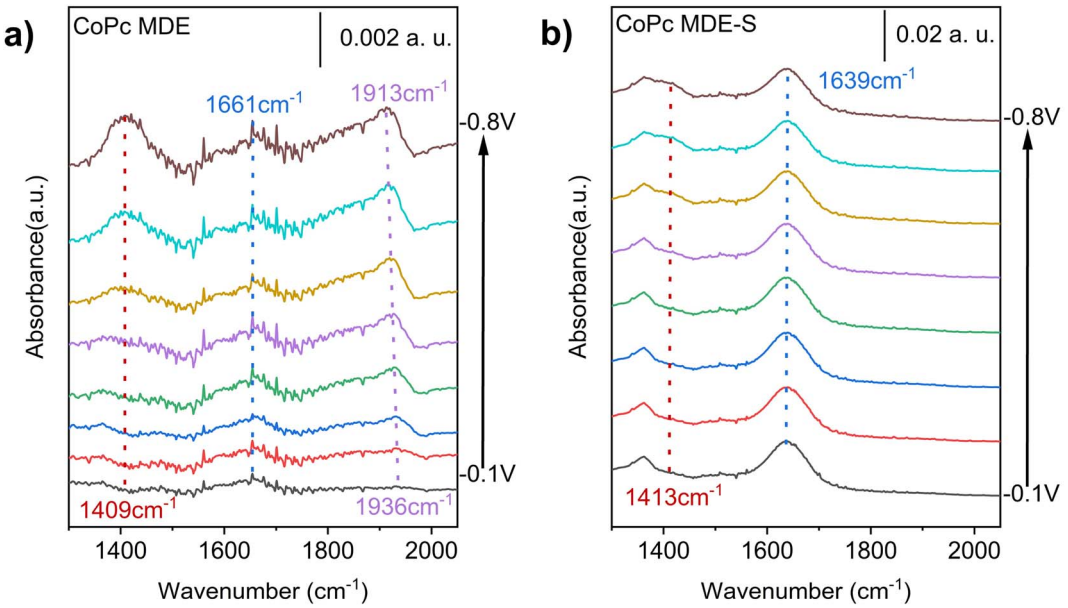

Fig. 8 *Operando* ATR-SEIRAS spectra of (a) CoPc MDE and (b) CoPc MDE-S obtained under stepped potential scans.

ionomers on the surface of CNTs and exposing the ionic groups of the ionomers. Due to the pronounced hydrophilicity of the ionic groups, the electrode surface became hydrophilic and the electrode microenvironment was significantly altered, thereby affecting the CO_2RR performance of CoPc MDE-S and CoPc MDE-P (Fig. 8). In contrast, the Ag electrodes exhibited relatively low sensitivity to the ionomers used because of the lack of such interactions between ionomer–Ag NPs.[60] Nano-graphite powder (NGP) with diameters of ~50 nm (Fig. S19†), which possessed similar morphology with Ag NPs but the same graphitic structures as CNTs, was chosen to verify the presence of π–π interactions between the anion-exchange ionomers with aromatic groups and CoPc MDE. The CO_2RR performance of NGP-CoPc MDE electrodes were shown in Table S2.† As expected, H_2 was the main product of NGP-CoPc MDE electrodes modified with anion-exchange ionomers like Sustainion and PiperION, while NGP-CoPc MDE-N electrodes exhibited superior CO_2RR performance. In addition, the contact angle of NGP-CoPc MDE-S and NGP-CoPc MDE-P exhibited similar results to those dispersed on CNTs. Raman spectroscopy was used to further examine the interactions between CNTs and the ionomer (Fig. S20†). Two distinct peaks were observed near ~1350 cm^{-1} and ~1584 cm^{-1}, corresponding to the D band and G band of CNTs, respectively. The G band peak of CoPc MDE-S was located at 1585.4 cm^{-1}, which showed a slight shift compared to CoPc MDE. This shift of the G band indirectly proved the modification of the Sustainion ionomer on CNTs.[58]

In order to prevent the degradation of catalyst performance, it is necessary to carefully select appropriate ionomer based on the nature of the catalyst due to the delicate interplay between ionomers and catalysts. Especially for catalysts with graphitic matrix, such as single-atom catalysts and dispersed molecular catalysts, the adverse interactions between aromatic groups in ionomers and the catalysts could lead to significant changes in the electrode microenvironment and subsequently result in a significant decrease in performance.

5. Conclusions

The addition of ionomers altered the surface morphology of GDEs and adjusted the electrode microenvironment. The different structures of ionomers and their interactions with the catalyst significantly modified the catalytic performance of the electrode. In the process of selecting ionomers, it was crucial to consider the potential interactions between the ionomer and the catalyst. Non-covalent interactions between ionomers and catalyst could significantly altered the hydrophilic and hydrophobic characteristics of the electrodes, disrupting the original three-phase boundary and increased selectivity of H_2. Through a comparative analysis of the impact of ionomers on Ag nanoparticles and CoPc MDE, the optimal ionomer–catalyst combinations achieved FE(CO) > 99% at current density up to −200 mA cm^{-2}. Furthermore, the long-term stability test of Ag and CoPc MDE-N exceeded 180 h at a current density of −100 mA cm^{-2}. The importance of selecting appropriate ionomers for the corresponding catalytic systems was identified. It was hoped that this work provided valuable insights into the selection of ionomers for future research in this field.

Data availability

Data supporting the findings of this study have been included as part of the ESI† and additional data are available from the corresponding authors upon reasonable request.

Author contributions

C. Yu and L. Xu prepared, characterized, and tested the catalysts. C. Yu, T. Lei, X. Zhang, and J. Yi wrote, review & editing the

manuscript. X. Zhang and X. Gao supervised this work. C. Yu, L. Xu, T. Lei, C. Jin, and X. Zhang conducted multiple formal analyses of the experimental results. All the authors discussed and commented on the manuscript.

Conflicts of interest

There are no conflicts of interest to declare.

Acknowledgements

This work was supported by National Key R&D Program of China (2023YFC3710800), Zhejiang Provincial Natural Science Foundation of China (LDT23E06012E06), Pioneer R&D Program of Zhejiang Province-China (2024SSYS0066, 2023C03016), and the National Energy-Saving and Low-Carbon Materials Production and Application Demonstration Platform Program (TC220H06N).

References

1 R. Xu, C. Hou, G. Xia, X. Sun, M. Li, H. Nie and D. Li, Effects of Ag promotion for Co/Al_2O_3 catalyst in Fischer-Tropsch synthesis, *Catal. Today*, 2020, **342**, 111–114.

2 H. Ma, Y. Yang, H. Fu, H. Zhang, W. Qian, Q. Sun and W. Ying, Effect of alkaline-earth metals (Mg, Ca, Sr, and Ba) on precipitated iron-based catalysts for high-temperature Fischer-Tropsch synthesis of light olefins, *Fuel*, 2024, **357**, 129605.

3 W. Zhang, J. Sun, H. Wang and X. Cui, Recent Advances in Hydrogenation of CO_2 to CO with Heterogeneous Catalysts Through the RWGS Reaction, *Chem.–Asian J.*, 2024, **19**(4), e202300971.

4 R. J. Lim, M. Xie, M. A. Sk, J.-M. Lee, A. Fisher, X. Wang and K. H. Lim, A review on the electrochemical reduction of CO_2 in fuel cells, metal electrodes and molecular catalysts, *Catal. Today*, 2014, **233**, 169–180.

5 S. Mou, Y. Li, L. Yue, J. Liang, Y. Luo, Q. Liu, T. Li, S. Lu, A. M. Asiri, X. Xiong, D. Ma and X. Sun, Cu2Sb decorated Cu nanowire arrays for selective electrocatalytic CO_2 to CO conversion, *Nano Res.*, 2021, **14**(8), 2831–2836.

6 J. Wang, J. Yu, M. Sun, L. Liao, Q. Zhang, L. Zhai, X. Zhou, L. Li, G. Wang, F. Meng, D. Shen, Z. Li, H. Bao, Y. Wang, J. Zhou, Y. Chen, W. Niu, B. Huang, L. Gu, C. S. Lee and Z. Fan, Surface Molecular Functionalization of Unusual Phase Metal Nanomaterials for Highly Efficient Electrochemical Carbon Dioxide Reduction under Industry-Relevant Current Density, *Small*, 2022, **18**(11), e2106766.

7 M. P. L. Kang, M. J. Kolb, F. Calle-Vallejo and B. S. Yeo, The Role of Undercoordinated Sites on Zinc Electrodes for CO_2 Reduction to CO, *Adv. Funct. Mater.*, 2022, **32**(23), 2111597.

8 L. Zhong, W. Pan, Z. Shi, C. Mao, J. Peng and J. Huang, Hollow Nitrogen-Doped porous carbon spheres decorated with atomically dispersed $Ni\text{-}N_3$ sites for efficient electrocatalytic CO_2 reduction, *J. Colloid Interface Sci.*, 2023, **649**, 571–580.

9 J. D. Yi, X. Gao, H. Zhou, W. Chen and Y. Wu, Design of Co-Cu Diatomic Site Catalysts for High-efficiency Synergistic CO_2 Electroreduction at Industrial-level Current Density, *Angew Chem. Int. Ed. Engl.*, 2022, **61**(47), e202212329.

10 Y. Dong, Q. Zhang, Z. Tian, B. Li, W. Yan, S. Wang, K. Jiang, J. Su, C. W. Oloman, E. L. Gyenge, R. Ge, Z. Lu, X. Ji and L. Chen, Ammonia Thermal Treatment toward Topological Defects in Porous Carbon for Enhanced Carbon Dioxide Electroreduction, *Adv. Mater.*, 2020, **32**(28), e2001300.

11 W. Liu, J. Qi, P. Bai, W. Zhang and L. Xu, Utilizing spatial confinement effect of N atoms in micropores of coal-based metal-free material for efficiently electrochemical reduction of carbon dioxide, *Appl. Catal., B*, 2020, **272**, e118974.

12 X. Wu, J. Y. Zhao, J. W. Sun, W. J. Li, H. Y. Yuan, P. F. Liu, S. Dai and H. G. Yang, Isolation of Highly Reactive Cobalt Phthalocyanine via Electrochemical Activation for Enhanced CO_2 Reduction Reaction, *Small*, 2023, **19**(23), e2207037.

13 Y. Song, J. J. Zhang, Y. Dou, Z. Zhu, J. Su, L. Huang, W. Guo, X. Cao, L. Cheng, Z. Zhu, Z. Zhang, X. Zhong, D. Yang, Z. Wang, B. Z. Tang, B. I. Yakobson, R. Ye and A. Thin, Ionic-Covalent Organic Nanosheets for Stable, High-Performance Carbon Dioxide Electroreduction, *Adv. Mater.*, 2022, **34**(42), e2110496.

14 Y. Jin, X. Zhan, Y. Zheng, H. Wang, X. Liu, B. Yu, X. Ding, T. Zheng, K. Wang, D. Qi and J. Jiang, In-situ growing nickel phthalocyanine supramolecular structure on carbon nanotubes for efficient electrochemical CO_2 conversion, *Appl. Catal., B*, 2023, **327**, e122446.

15 X. Zhang, Y. Wang, M. Gu, M. Wang, Z. Zhang, W. Pan, Z. Jiang, H. Zheng, M. Lucero, H. Wang, G. E. Sterbinsky, Q. Ma, Y.-G. Wang, Z. Feng, J. Li, H. Dai and Y. Liang, Molecular engineering of dispersed nickel phthalocyanines on carbon nanotubes for selective CO2 reduction, *Nat. Energy*, 2020, **5**(9), 684–692.

16 J. R. Huang, X. F. Qiu, Z. H. Zhao, H. L. Zhu, Y. C. Liu, W. Shi, P. Q. Liao and X. M. Chen, Single-Product Faradaic Efficiency for Electrocatalytic of CO_2 to CO at Current Density Larger than 1.2 A cm^{-2} in Neutral Aqueous Solution by a Single-Atom Nanozyme, *Angew Chem. Int. Ed. Engl.*, 2022, **61**(44), e202210985.

17 X. Zhang, J. Li, Y. Y. Li, Y. Jung, Y. Kuang, G. Zhu, Y. Liang and H. Dai, Selective and High Current CO_2 Electro-Reduction to Multicarbon Products in Near-Neutral KCl Electrolytes, *J. Am. Chem. Soc.*, 2021, **143**(8), 3245–3255.

18 T. Moore, X. Xia, S. E. Baker, E. B. Duoss and V. A. Beck, Elucidating Mass Transport Regimes in Gas Diffusion Electrodes for CO_2 Electroreduction, *ACS Energy Lett.*, 2021, **6**(10), 3600–3606.

19 A. Senocrate, F. Bernasconi, D. Rentsch, K. Kraft, M. Trottmann, A. Wichser, D. Bleiner and C. Battaglia, Importance of Substrate Pore Size and Wetting Behavior in Gas Diffusion Electrodes for CO_2 Reduction, *ACS Appl. Energy Mater.*, 2022, **5**(11), 14504–14512.

20 S. B. Dolmanan, A. Böhme, Z. Fan, A. J. King, A. Q. Fenwick, A. D. Handoko, W. R. Leow, A. Z. Weber, X. Ma, E. Khoo,

H. A. Atwater and Y. Lum, Local microenvironment tuning induces switching between electrochemical CO_2 reduction pathways, *J. Mater. Chem. A*, 2023, **11**(25), 13493–13501.

21 Z. Xing, L. Hu, D. S. Ripatti, X. Hu and X. Feng, Enhancing carbon dioxide gas-diffusion electrolysis by creating a hydrophobic catalyst microenvironment, *Nat. Commun.*, 2021, **12**(1), 136.

22 M. Chang, W. Ren, W. Ni, S. Lee and X. Hu, Ionomers Modify the Selectivity of Cu-Catalyzed Electrochemical CO_2 Reduction, *ChemSusChem*, 2023, **16**(5), e202201687.

23 C. Kim, J. C. Bui, X. Luo, J. K. Cooper, A. Kusoglu, A. Z. Weber and A. T. Bell, Tailored catalyst microenvironments for CO_2 electroreduction to multicarbon products on copper using bilayer ionomer coatings, *Nat. Energy*, 2021, **6**(11), 1026–1034.

24 M. Esmaeilirad, A. Kondori, N. Shan, M. T. Saray, S. Sarkar, A. M. Harzandi, C. M. Megaridis, R. Shahbazian-Yassar, L. A. Curtiss, C. U. Segre and M. Asadi, Efficient electrocatalytic conversion of CO_2 to ethanol enabled by imidazolium-functionalized ionomer confined molybdenum phosphide, *Appl. Catal., B*, 2022, **317**, e121681.

25 X. Du, P. Zhang, G. Zhang, H. Gao, L. Zhang, M. Zhang, T. Wang and J. Gong, Confinement of ionomer for electrocatalytic CO_2 reduction reaction via efficient mass transfer pathways, *Natl. Sci. Rev.*, 2024, **11**(2), nwad149.

26 X. Zhang, Z. Wu, X. Zhang, L. Li, Y. Li, H. Xu, X. Li, X. Yu, Z. Zhang, Y. Liang and H. Wang, Highly selective and active CO_2 reduction electrocatalysts based on cobalt phthalocyanine/carbon nanotube hybrid structures, *Nat. Commun.*, 2017, **8**, 14675.

27 H.-L. Zhu, Y.-Q. Zheng and M. Shui, Synergistic Interaction of Nitrogen-Doped Carbon Nanorod Array Anchored with Cobalt Phthalocyanine for Electrochemical Reduction of CO_2, *ACS Appl. Energy Mater.*, 2020, **3**(4), 3893–3901.

28 X. Peng, S. G. Karakalos and W. E. Mustain, Preferentially Oriented Ag Nanocrystals with Extremely High Activity and Faradaic Efficiency for CO_2 Electrochemical Reduction to CO, *ACS Appl. Mater. Interfaces*, 2018, **10**(2), 1734–1742.

29 W. Guo, K. Shim, F. O. Odongo Ngome, Y. H. Moon, S.-Y. Choi and Y.-T. Kim, Highly active coral-like porous silver for electrochemical reduction of CO_2 to CO, *J. CO2 Util.*, 2020, **41**, e101242.

30 M. Ma, K. Liu, J. Shen, R. Kas and W. A. Smith, In Situ Fabrication and Reactivation of Highly Selective and Stable Ag Catalysts for Electrochemical CO_2 Conversion, *ACS Energy Lett.*, 2018, **3**(6), 1301–1306.

31 M. Takasaki, K. Kimura, K. Kawaguchi, A. Abe and G. Katagiri, Structural Analysis of a Perfluorosulfonate Ionomer in Solution by 19F and 13C NMR, *Macromolecules*, 2005, **38**(14), 6031–6037.

32 T. Agarwal, A. K. Prasad, S. G. Advani, S. K. Babu and R. L. Borup, Infrared spectroscopy for understanding the structure of Nafion and its associated properties, *J. Mater. Chem. A*, 2024, **12**(24), 14229–14244.

33 Z. Liu, H. Yang, R. Kutz and R. I. Masel, CO_2 Electrolysis to CO and O_2 at High Selectivity, Stability and Efficiency Using Sustainion Membranes, *J. Electrochem. Soc.*, 2018, **165**(15), J3371.

34 R. B. Kutz, Q. Chen, H. Yang, S. D. Sajjad, Z. Liu and I. R. Masel, Sustainion Imidazolium-Functionalized Polymers for Carbon Dioxide Electrolysis, *Energy Technol.*, 2017, **5**(6), 929–936.

35 J. Wang, Y. Zhao, B. P. Setzler, S. Rojas-Carbonell, C. Ben Yehuda, A. Amel, M. Page, L. Wang, K. Hu, L. Shi, S. Gottesfeld, B. Xu and Y. Yan, Poly(aryl piperidinium) membranes and ionomers for hydroxide exchange membrane fuel cells, *Nat. Energy*, 2019, **4**(5), 392–398.

36 S. Chang, Y. Xuan, J. Duan and K. Zhang, High-performance electroreduction CO_2 to formate at Bi/Nafion interface, *Appl. Catal., B*, 2022, **306**, e121135.

37 M. Liu, H. Hu, Y. Kong, I. Z. Montiel, V. Kolivoška, A. V. Rudnev, Y. Hou, R. Erni, S. Vesztergom and P. Broekmann, The role of ionomers in the electrolyte management of zero-gap MEA-based CO_2 electrolysers: A Fusion vs. Nafion comparison, *Appl. Catal., B*, 2023, **335**, e122855.

38 H. Park, P. N. Shah, H. M. Tee and P. A. Kohl, Self-adhesive ionomers for alkaline electrolysis: Optimized oxygen evolution electrode, *J. Power Sources*, 2023, **564**, e232811.

39 B. Wang, J. Pan, X. Zou, J. Zhao, G. Xu, Z. Jin, Z. Sun and F. Yan, UV-crosslinkable anthracene-based ionomer derived gas "Expressway" for anion exchange membrane fuel cells, *J. Mater. Chem. A*, 2022, **10**(25), 13355–13367.

40 Y.-C. Park, H. Tokiwa, K. Kakinuma, M. Watanabe and M. Uchida, Effects of carbon supports on Pt distribution, ionomer coverage and cathode performance for polymer electrolyte fuel cells, *J. Power Sources*, 2016, **315**, 179–191.

41 Y.-C. Park, K. Kakinuma, H. Uchida, M. Watanabe and M. Uchida, Effects of short-side-chain perfluorosulfonic acid ionomers as binders on the performance of low Pt loading fuel cell cathodes, *J. Power Sources*, 2015, **275**, 384–391.

42 M. Ma, E. L. Clark, K. T. Therkildsen, S. Dalsgaard, I. Chorkendorff and B. Seger, Insights into the carbon balance for CO_2 electroreduction on Cu using gas diffusion electrode reactor designs, *Energy Environ. Sci.*, 2020, **13**(3), 977–985.

43 S. Liu, H. Tao, L. Zeng, Q. Liu, Z. Xu, Q. Liu and J. L. Luo, Shape-Dependent Electrocatalytic Reduction of CO_2 to CO on Triangular Silver Nanoplates, *J. Am. Chem. Soc.*, 2017, **139**(6), 2160–2163.

44 S. Liu, X.-Z. Wang, H. Tao, T. Li, Q. Liu, Z. Xu, X.-Z. Fu and J.-L. Luo, Ultrathin 5-fold twinned sub-25 nm silver nanowires enable highly selective electroreduction of CO_2 to CO, *Nano Energy*, 2018, **45**, 456–462.

45 Y. Wu, Z. Jiang, X. Lu, Y. Liang and H. Wang, Domino electroreduction of CO_2 to methanol on a molecular catalyst, *Nature*, 2019, **575**(7784), 639–642.

46 E. Boutin, M. Wang, J. C. Lin, M. Mesnage, D. Mendoza, B. Lassalle-Kaiser, C. Hahn, T. F. Jaramillo and M. Robert, Aqueous Electrochemical Reduction of Carbon Dioxide and Carbon Monoxide into Methanol with Cobalt

Phthalocyanine, *Angew Chem. Int. Ed. Engl.*, 2019, **58**(45), 16172–16176.

47 D. Wakerley, S. Lamaison, F. Ozanam, N. Menguy, D. Mercier, P. Marcus, M. Fontecave and V. Mougel, Bio-inspired hydrophobicity promotes CO_2 reduction on a Cu surface, *Nat. Mater.*, 2019, **18**(11), 1222–1227.

48 Y. Jiang, D. Zhong, L. Wang, J. Li, G. Hao, J. Li and Q. Zhao, Roughness Effect of Cu on Electrocatalytic CO_2 Reduction towards C_2H_4, *Chem.–Asian J.*, 2022, **17**(14), e202200380.

49 Z. Xing, X. Hu and X. Feng, Tuning the Microenvironment in Gas-Diffusion Electrodes Enables High-Rate CO_2 Electrolysis to Formate, *ACS Energy Lett.*, 2021, **6**(5), 1694–1702.

50 F. Bienen, D. Kopljar, S. Geiger, N. Wagner and K. A. Friedrich, Investigation of CO_2 Electrolysis on Tin Foil by Electrochemical Impedance Spectroscopy, *ACS Sustain. Chem. Eng.*, 2020, **8**(13), 5192–5199.

51 M. E. Leonard, L. E. Clarke, A. Forner-Cuenca, S. M. Brown and F. R. Brushett, Investigating Electrode Flooding in a Flowing Electrolyte, Gas-Fed Carbon Dioxide Electrolyzer, *ChemSusChem*, 2020, **13**(2), 400–411.

52 N. J. Firet and W. A. Smith, Probing the Reaction Mechanism of CO_2 Electroreduction over Ag Films via Operando Infrared Spectroscopy, *ACS Catal.*, 2016, **7**(1), 606–612.

53 N. Meng, W. Zhou, Y. Yu, Y. Liu and B. Zhang, Superficial Hydroxyl and Amino Groups Synergistically Active Polymeric Carbon Nitride for CO_2 Electroreduction, *ACS Catal.*, 2019, **9**(12), 10983–10989.

54 Y. Li, S. Xie, X. Huang, W. Song, C. Chen, H. Sheng and J. Zhao, Spectating the proton migration on catalyst with noninnocent ligand in aqueous electrochemical CO_2 reduction, *Appl. Catal., B*, 2023, **329**, e122542.

55 X. Ren, J. Zhao, X. Li, J. Shao, B. Pan, A. Salame, E. Boutin, T. Groizard, S. Wang, J. Ding, X. Zhang, W. Y. Huang, W. J. Zeng, C. Liu, Y. Li, S. F. Hung, Y. Huang, M. Robert and B. Liu, In-situ spectroscopic probe of the intrinsic structure feature of single-atom center in electrochemical CO/CO_2 reduction to methanol, *Nat. Commun.*, 2023, **14**(1), 3401.

56 Y.-G. Yan, Q.-X. Li, S.-J. Huo, M. Ma, W.-B. Cai and M. Osawa, Ubiquitous Strategy for Probing ATR Surface-Enhanced Infrared Absorption at Platinum Group Metal–Electrolyte Interfaces, *J. Phys. Chem. B*, 2005, **109**(16), 7900–7906.

57 S. Wang, X. Wang and S. P. Jiang, PtRu Nanoparticles Supported on 1-Aminopyrene-Functionalized Multiwalled Carbon Nanotubes and Their Electrocatalytic Activity for Methanol Oxidation, *Langmuir*, 2008, **24**(18), 10505–10512.

58 X. Qi, K. Y. Pu, X. Zhou, H. Li, B. Liu, F. Boey, W. Huang and H. Zhang, Conjugated-polyelectrolyte-functionalized reduced graphene oxide with excellent solubility and stability in polar solvents, *Small*, 2010, **6**(5), 663–669.

59 T. Fujigaya and N. Nakashima, Fuel cell electrocatalyst using polybenzimidazole-modified carbon nanotubes as support materials, *Adv. Mater.*, 2013, **25**(12), 1666–1681.

60 S. A. Berlinger, B. D. McCloskey and A. Z. Weber, Inherent Acidity of Perfluorosulfonic Acid Ionomer Dispersions and Implications for Ink Aggregation, *J. Phys. Chem. B*, 2018, **122**(31), 7790–7796.

